Electronic Supplementary Material (ESI) for ChemComm.

An N-ethylated barbituric acid end-capped bithiophene as an electron-acceptor material in fullerene-free organic photovoltaics

Paul Sullivan,[a*] Gavin E. Collis,[b*] Luke A. Rochford,[a] Junior Ferreira Arantes,[b] Peter Kemppinen,[b] Tim S. Jones,[a] and Kevin N. Winzenberg.[b]

[a]Department of Chemistry, University of Warwick, Coventry, CV4 7AL, UK
[b]CSIRO Manufacturing Flagship, Advanced Fibres and Chemical Industries, Private Bag 10, Clayton South MDC, VIC, 3169, Australia

*Corresponding authors, E-mail: p.j.sullivan@warwick.ac.uk and Gavin.Collis@csiro.au

Supplementary Information

Contents

1. Materials 2
2. Film and Device Fabrication 2
3. UV/Visible and Photoluminescene studies 2
4. Electron Mobility 3
5. Atomic force microscopy (AFM) studies 4
6. X-ray diffraction (XRD) studies 5
7. OPV Devices 6
8. References 8

1. Materials

EBB was synthesised and purified, by sublimation, as previously reported.[1] All other materials were obtained commercially and used as received: boron subphthalocyanine chloride (SubPc, Luminescence Technology Corp., sublimed grade), Zirconium(IV) acetylacetonate (Zr(acac), Aldrich), molybdenum oxide (MoO_x, Aldrich), bathocuproine (BCP, Aldrich), N,N′-Di(1-naphthyl)-N,N′-diphenyl-(1,1′-biphenyl)-4,4′-diamine (NPD, Aldrich).

2. Film and Device Fabrication

All evaporated films and devices were produced in a Kurt J. Lesker Spectros multi-source evaporation system with a base pressure of ~$5x10^{-8}$ mbar and *in-situ* shadow masking. Growth rate and thickness were monitored by a series of quartz crystal microbalances, with independent source monitoring allowing accurate control of the composition of codeposited layers. All devices, structures for mobility measurements, and samples for XRD analysis were grown on custom patterned indium-doped tin oxide (ITO, <15 Ω/□) coated glass substrates (Thin Film Devices Inc.) which were cleaned by successive detergent, solvent and UV-Ozone steps. Structures for PL quenching and transmissive geometry absorption measurements were produced on quartz substrates following the same cleaning procedure as above. Zr(acac) layers were produced by spin-coating a 1 mg/ml solution in isopropanol in ambient conditions with no post-fabrication annealing step. Devices were completed by the evaporation of an aluminium top contact through a shadow mask to produce an active area of 0.2 cm^2. OPV devices were subsequently capped with 50nm of MoO_x as a protective layer before being removed directly to a nitrogen-filled glovebox for encapsulation with a UV-cured epoxy (Ossila Ltd.) and glass coverslip.

3. UV/Visible and Photoluminescene studies

Absorption measurements, in both transmissive and reflective geometry, were recorded on the same custom system as the EQE measurements (described in more detail in the Electrical Characterisation part of section 7) using the split beams as reference and sample paths (after initial calibration) and the photodiodes as movable detectors to allow the different geometries.

Photoluminescence Quenching (PL) measurements were recorded using a customised Horiba FluoroLog-3 Spectrofluorometer. Here PL emission scans are performed whilst selectively exciting a material both with and without a second dissociating layer. Any reduction in emission on adding the dissociating layer is indicative of the formation of an additional non-radiative exciton decay pathway which can be attributed to exciton dissociation, and charge generation, at the material interface. In planar junction structures, where the exciton diffusion length is important, quenching ratios in the range 40-60 % tend to demonstrate strong dissociation. Samples were illuminated through the quartz

substrate directly into the material to be excited to ensure a consistent substrate/organic interface for PL collection. Light intensity, slit widths, and incidence/collection angles were also kept constant between scans to ensure the collected absolute intensity measurements provided a measure of relative PL quantum yield.

4. Electron Mobility

Electron mobility was calculated for the EBB films through the trap-free space-charge-limited current (SCLC) model whereby the space-charge limited current density (J) can be expressed as a function of the applied bias (V) by the Mott–Gurney equation:

$$J = \frac{9}{8}\varepsilon\varepsilon_0\mu\frac{V^2}{d^3}$$

where ε is the relative dielectric constant of the material (is this case we assume a value of $\varepsilon = 3$), ε_0 is the permittivity of free space, μ is the charge carrier mobility and d is the film thickness.[2] The fitting allowed for a Poole-Frenkel electric field dependence typical of most organic thin films whereby the mobility is expressed as:

$$\mu(E) = \mu_0 \exp[\gamma\sqrt{E}]$$

This field dependence arises from the disordered nature of the films which leads to transport via a hopping mechanism between sites with a random variation in energy. This energy variation causes small energy barriers to charge transport which can be overcome by the electric field.

To ensure the determination of electron mobility, electron-only sandwich devices with charge selective contacts are required. Zr(acac) has been shown as an efficient electron-transport material,[3] whilst the work function of Al is matched closely to that of the LUMO of EBB, hence a structure of ITO / Zr(acac) / EBB (100 nm) / Al (200 nm) was used. Fitting of a J-V curve of this structure (Figure S1) produced values of the zero-field electron mobility of $\mu_0 = 1.25\text{x}10^{-7}$ cm^2 V^{-1} s^{-1} and the field activation parameter of $\gamma = 3.73 \text{ x } 10^{-4}$ [cm V^{-1}]$^{1/2}$.

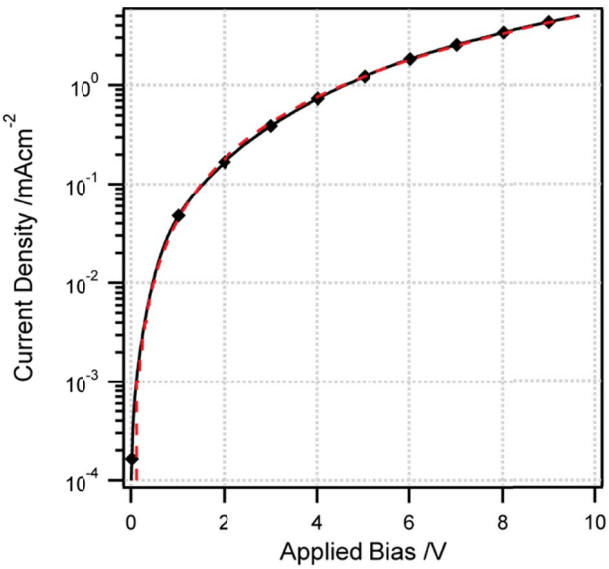

Figure S1: *J-V* curve of an electron-only device of structure ITO / Zr(acac) / EBB (100 nm) / Al (200 nm) (black line, filled diamonds) along with a Mott-Gurney fit (red dashed line) allowing the calculation of an electron mobility of $\mu_0 = 1.25 \times 10^{-7}$ cm^2 V^{-1} s^{-1}.

5. Atomic force microscopy (AFM) studies

Atomic force microscopy (AFM) images were obtained from an Asylum Research MFP-3D in AC (tapping) mode. The EBB formed relatively rough, soft surfaces which were challenging to characterise, hence the relatively poor images obtained. However, the general topology and roughness is clearly visible and is comparable when grown both directly on ITO and onto a Zr(acac) interlayer.

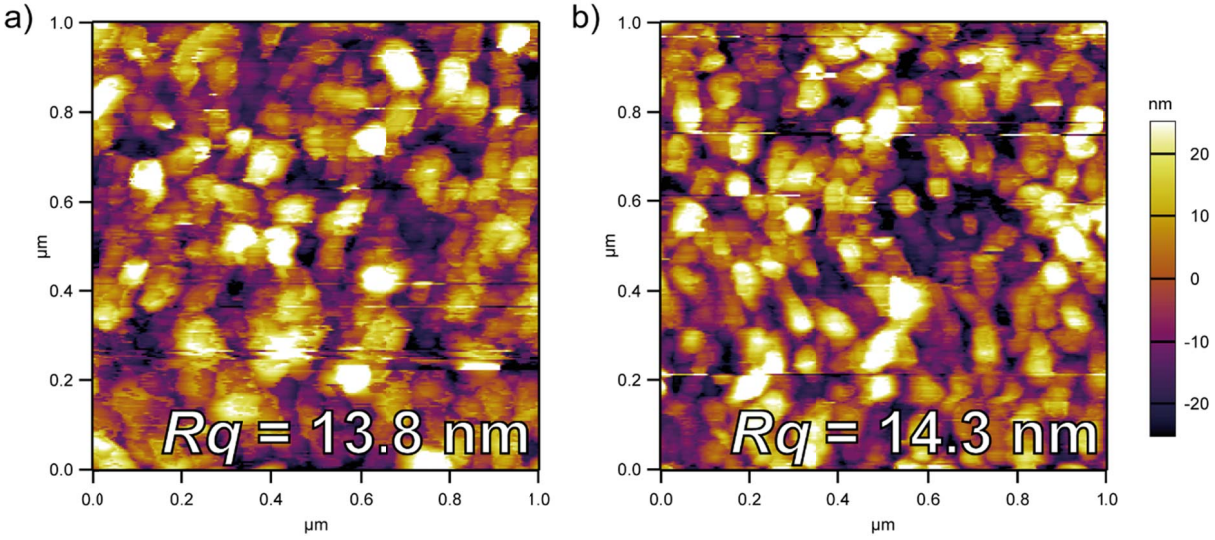

Figure S2: Tapping mode AFM images of 50 nm EBB layers grown (a) directly on ITO and (b) onto a Zr(acac) buffer layer. The images share a common z-scale.

6. X-ray diffraction (XRD) studies

Thin film XRD patterns were obtained using a Panalytical X'Pert Pro MRD diffractometer with monochromatic Cu $K\alpha_1$ radiation. In all cases the EBB was grown to a layer thickness of ~90 nm, with the SubPc interlayer grown to 20 nm. Evaporated films of SubPc generally show no diffraction peaks.[4]

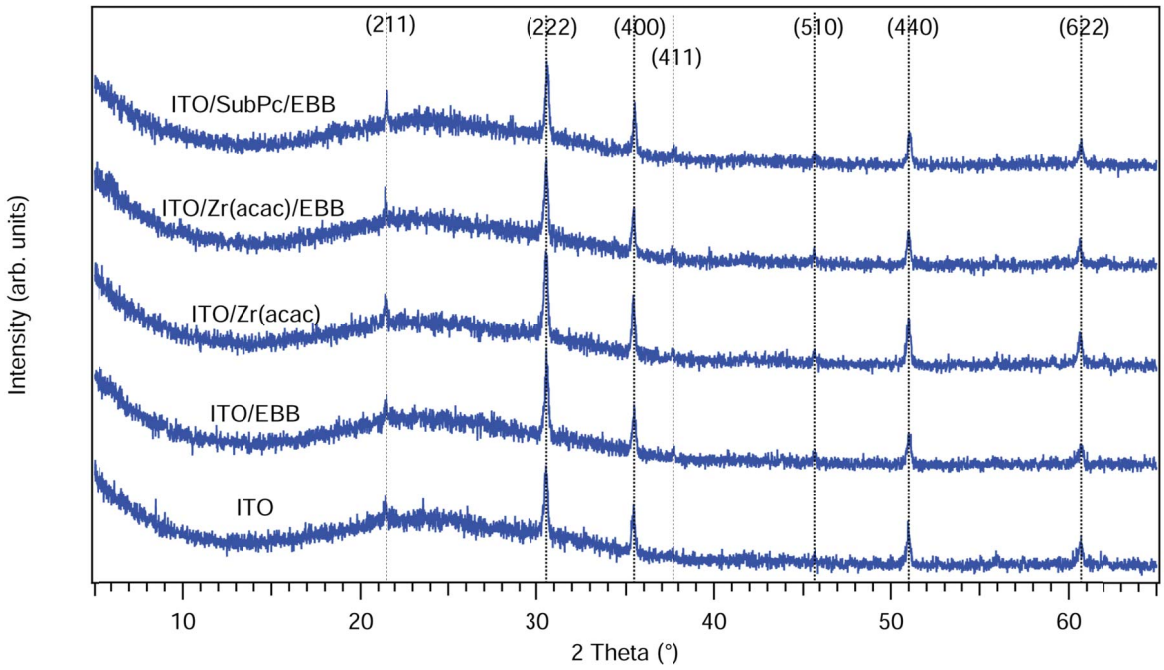

Figure S3: XRD traces of single layers of Zr(acac) and EBB, and bilayers of Zr(acac)/EBB and SubPc/EBB all produced on ITO substrates. All visible peaks can be assigned to the underlying ITO substrate.

7. OPV Devices

Band Diagrams of Regular and Inverted Structures

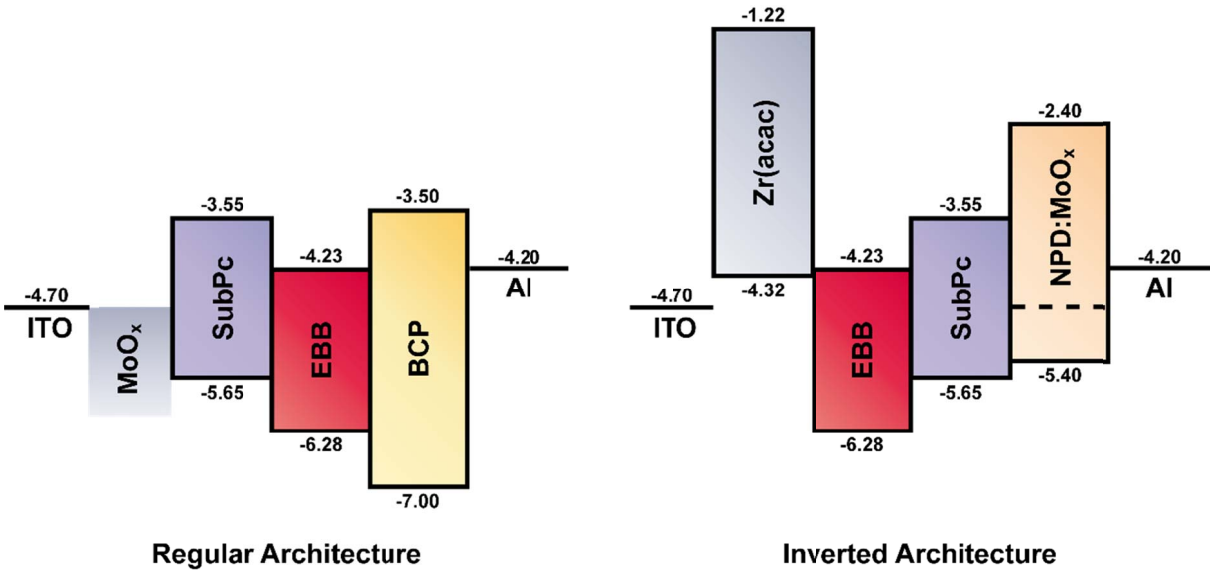

Figure S4: Energy level diagrams of the regular and inverted architecture devices. Frontier orbital energies for the active materials were taken from the literature.[1, 3, 5] MoO_x is believed to transport holes via mid-gap states, and thus the level is not defined precisely.[6, 7]

Electrical Characterisation

J-V curves were recorded with a Keithley 2400 sourcemeter controlled from a custom LabVIEW interface. All illuminated *J-V* curves were measured under light from a Newport Oriel Class AAA solar simulator with intensity tuned to within 0.5% of 1 sun (100 mW cm^{-2}) using a calibrated silicon photodiode with KG-5 filter to aid spectral matching. The *J-V* curves for the inverted devices were recorded after a positive burn-in period of ~10 minutes when performance was optimised. Curves and parameters were corrected to precisely 1 sun based on the actual measured light intensity before being averaged over 4 pixels (regular architecture devices) or 12 pixels (inverted architecture devices). External quantum efficiency (EQE) measurements were performed on a custom-built system employing mechanically chopped, monochromatic light from a xenon arc lamp source. Two calibrated, UV-enhanced silicon photodiodes (Newport 818-UV) were employed, the first as a reference diode, the second as a calibration diode which was measured during both reference and sample scans *via* a split beam to correct for fluctuations in light intensity between scans. Current signals were passed through custom built high-gain, low-noise transimpedance amplifiers before being recorded by a National Instruments NI USB-4431 DAQ board. Multichannel lock-in amplification was performed by a custom LabVIEW interface which also processed and recorded measured data. The EQE curves presented are from single pixel measurements corrected to account

for the difference between the measured pixel J_{SC} and the averaged J_{SC} of the particular device structure. Pixels with measured J_{SC} values close to the average J_{SC} were selected for EQE measurements ensuring correction factors of <3%.

Performance Parameters

Architecture (layer varied)	**Layer Thickness /nm**	J_{SC} **/mA cm^{-2}**	V_{OC} **/V**	***FF***	**Efficiency /% (best pixel)**
Regular (EBB)	20	2.34	1.38	0.40	1.28 (1.32)
	40	1.86	1.35	0.30	0.76 (0.85)
Inverted (NPD:MoO$_x$)	10	3.43	1.25	0.48	1.99 (2.12)
	20	3.85	1.24	0.50	2.39 (2.57)
	30	3.72	1.28	0.49	2.33 (2.40)
	40	3.59	1.28	0.45	2.07 (2.17)
	50	3.21	1.28	0.47	1.91 (1.99)

Table S1: Key parameters for all reported devices. Regular architecture: ITO / MoOx (5 nm) / SubPc (15 nm) / EBB (20 or 40 nm) / BCP (8 nm) / Al (200 nm) (4 pixels averaged), Inverted architecture: ITO / Zr(acac) / EBB (20 nm) / SubPc (20 nm) / NPD:MoOx (6:1, 10-50 nm) / Al (200 nm) (12 pixels averaged).

8. References

1. Y. Shu, A. Mikosch, K. N. Winzenberg, P. Kemppinen, C. D. Easton, A. Bilic, C. M. Forsyth, C. J. Dunn, T. B. Singh and G. E. Collis, *J. Mater. Chem. C*, 2014, **2**, 3895-3899.
2. V. D. Mihailetchi, J. K. J. van Duren, P. W. M. Blom, J. C. Hummelen, R. A. J. Janssen, J. M. Kroon, M. T. Rispens, W. J. H. Verhees and M. M. Wienk, *Adv. Funct. Mater.*, 2003, **1**, 43-46.
3. Z. Tan, S. Li, F. Wang, D. Qian, J. Lin, J. Hou and Y. Li, *Sci. Rep.*, 2014, **4**, 4691.
4. R. R. Lunt, N. C. Giebink, A. A. Belak, J. B. Benziger and S. R. Forrest, *J. Appl. Phys.*, 2009, **105**, 053711.
5. N. Beaumont, S. W. Cho, P. Sullivan, D. Newby, K. E. Smith and T. S. Jones, *Adv. Funct. Mater.*, 2012, **22**, 561.
6. K. Kanai, K. Koizumi, S. Ouchi, Y. Tsukamoto, K. Sakanoue, Y. Ouchi and K. Seki, *Org. Electron.*, 2010, **11**, 188-194.
7. I. Hancox, P. Sullivan, K. V. Chauhan, N. Beaumont, L. A. Rochford, R. A. Hatton and T. S. Jones, *Org. Electron.*, 2010, **11**, 2019–2025.